ADVANCED OPTICAL MATERIALS
www.advopticalmat.de

Direct Imprint of Optical Functionalities on Free-Form Chalcogenide Glasses

*Natali Ostrovsky, Dor Yehuda, Sivan Tzadka, Evyatar Kassis, Shay Joseph, and Mark Schvartzman**

Scalable surface patterning of chalcogenide glasses is the crux for many optical applications of these promising optical materials. Here, a novel, resist-free surface patterning of chalcogenide glasses with 3D relief microstructures is introduced, using direct radiation-assisted thermal imprint. The imprint is based on a nanocomposite mold made of a carbon nanotube matrix and polydimethylsiloxane resin. To allow nanoimprint, the mold and glass substrate are confined between two elastic membranes, pneumatically pressed against each other, and controllably radiated by an infrared bulb. Since chalcogenide glass is transparent to infrared radiation, the radiation is mostly absorbed in the mold due to the embedded carbon nanotubes, so that the glass–mold interface is heated to the imprint temperature. By using this approach, the first of its type direct imprint of chalcogenide glass of any arbitrary form is demonstrated, including flat substrates and convex aspheric lenses. The composition and structure of imprinted chalcogenide glass are analyzed, and it is demonstrated that they are well maintained throughout the imprint. It is optically characterized both in transmission and reflection modes. It is believed that the innovation provides a quantum leap in the micro- and nanoscale processing of chalcogenide glasses, and opens the pathway to their numerous applications.

Chalcogenide glasses—amorphous chemical compounds that contain one or more chalcogens (Sulfur, Selenium, or Tellurium)—are attractive materials for optical applications.[1–3] They have a high refractive index and high transmittance in the visible to mid-infrared region—both can be easily tailored by glass composition.[4] Due to these properties, chalcogenide glasses are broadly used in various components for infrared optics, such as fibers, waveguides, and lenses. In addition, chalcogenide glassed have been known for their strong third-order optical nonlinearity due to the low phonon energy of the bonds between heavy chalcogen atoms, and thus are very attractive for all-optical switching.[5] Also, chalcogenide glasses can change their phase upon interaction with electrons,[6] X-rays,[7] and photons whose energy is larger than the glass bandgap.[8] The latter type of phase transformation makes chalcogenide glasses attractive for non-volatile memory devices.[9]

One important aspect of the fabrication of many optical devices is surface pattering with miniaturized functional structures, for example, waveguides, resonators, or diffraction grating. To pattern chalcogenide glasses for device fabrication, direct writing with an electron beam or with a laser has been broadly used.[10–12] However, beam writing, which is a serial process, has a very low throughput, and is thus suitable for prototyping rather than for scalable fabrication of devices. Alternatively, parallel micropatterning of chalcogenide glasses is possible by holographic recording,[13] as well as by photolithography in both binary and grayscale modes.[8,14] Yet, these fabrication approaches can be applied to flat surfaces only. At the same time, numerous applications of chalcogenide glasses require patterning of curved optical surfaces, such as lenses, with functional micropatterns, for example, diffraction grating or with moth-eye antireflective morphologies. However, scalable pattering of curved surfaces of chalcogenide glasses has not been demonstrated to date.

All the abovementioned limitations of the state-of-the-art micro-/nano-patterning approaches can, in principle, be overcome by soft imprint. Soft imprint, which is based on the mechanical embossing of an elastomeric mold into a material heated above its glass transition temperature, has been broadly used to pattern thin films of UV-curable polymers.[15] Due to the mechanical flexibility of soft molds, soft imprint can produce high-resolution nanostructures in UV curable polymer films deposited on substrates with unconventional geometry, such as lenses and optical fibers.[16] Furthermore, our group has recently demonstrated thermal nanoimprint of polymer films on both flat surfaces and lenses.[17,18] There, the imprint temperature was chosen to be sufficiently above the glass transition point of the imprinted polymer to ensure its viscous flow, yet still below the temperature at which the mold can be damaged.

N. Ostrovsky, D. Yehuda, S. Tzadka, Dr. M. Schvartzman
Department of Materials Engineering
Isle Katz Institute of Nanoscale Science and Technology
Ben-Gurion University of the Negev
Beer-Sheva 8410501, Israel
E-mail: marksc@bgu.ac.il
E. Kassis, S. Joseph
Optical Component Center
RAFAEL
Haifa 3102102, Israel
The ORCID identification number(s) for the author(s) of this article can be found under https://doi.org/10.1002/adom.201900652.

DOI: 10.1002/adom.201900652

Similarly to organic polymers, many chalcogenide glasses have a relatively low glass transition temperature, for example, 163 °C for $GeSe_4$ or 185 °C for As_2S_3.[19] Thus, many chalcogenide glasses can, in principle, be imprinted with soft molds. To date, soft imprint was demonstrated for chalcogenide glasses such as $As_{24}Se_{36}S_{36}$,[20] As_2S_3,[21] and As_2Se_3,[22,23] yet it was limited to thin films of these materials deposited onto hard Silicon substrates, but not onto bulk chalcogenide substrates. The reason for which bulk chalcogenide glasses cannot be directly patterned by a conventional imprint approach is that the high pressure and temperature required for the surface imprint will also cause the global deformation of the entire substrate. Imprint the surface without deforming the bulk substrate still remains a great challenge. Direct imprint of bulk chalcogenide glasses without applying an external pressure does not deform the bulk substrate; however, it results in an incomplete pattern transfer from the mold to the glass surface.[24] Recently, direct imprint of chalcogenide glass was also demonstrated by confining the substrate within a tight metallic fixture that prevents substrate deformation.[18,25,26] Yet, the flatness of the imprinted substrate was not quantified in these reports. Also, confinement-based imprint requires a precisely machined fixture custom-fitted for each type of the imprinted substrate, and is limited to planar substrates only.

Here, we introduce a novel approach for the direct surface imprint of chalcogenide glasses. Our approach is based on the radiative heating of the interface between the glass and soft mold (**Figure 1**). To facilitate the effective mold heating by radiation, we produced the mold from a composite material of Polydimethylsiloxane (PDMS) and multi-wall carbon nanotubes, by casting the PDMS-nanotube mixture onto a photolithographically fabricated master followed by thermal curing. We used this mold to directly imprint the surface of As_2Se_3—a chalcogenide glass whose glass transition temperature is about 185 °C.[27] To that end, we sealed the sandwiched mold and glass between two transparent membranes, heated the carbon-nanotube reinforced mold by infrared radiative source, and pneumatically pressurized them. This new imprint methodology, together with appropriately chosen process conditions, ensured that only a thin layer at the mold-glass interface was sufficiently heated above the As_2Se_3 glass transition point. As a result of this highly localized heating, a viscous flow of As_2Se_3 is developed near its interface with the mold, whereas the rest of the glass substrate does not deform during the imprint. Indeed, using this approach, we demonstrated the full pattern transfer from the mold to the surface of chalcogenide glass, while maintaining the glass substrate completely undistorted. To verify that the composition and structure of the chalcogenide glass is maintained throughout the imprint process, we performed a series of surface analysis of the imprinted glass, including Raman Spectroscopy, Energy-dispersive X-ray Spectroscopy (EDS), X-Ray Photoelectron Spectroscopy (XPS), and X-Ray Diffraction (XRD). We also found that the complete flatness of the imprinted substrate can be achieved by using a mechanical support to its back side. To illustrate the applicability of our approach in the fabrication of optical devices, we produced a 2D diffraction grating, and characterized it in both reflection and transmission modes. Finally, we demonstrated, for the first time to the best of our knowledge, imprint of chalcogenide glasses with a non-planar geometry, by producing a diffraction grating on an aspherical lens of As_2Se_3. We believe, that all these innovations and findings address key challenges in the micro-processing of chalcogenide glasses, and pave the way to future optical devices and systems based on this promising family of materials.

The pattern we used to demonstrate our novel imprint approach consisted of a 2D diffraction grating with a periodicity of 10 µm. To fabricate soft molds with this pattern, we first produced a master mold by photolithography. For this purpose, we patterned a film of photoresist on a Si substrate, and used it directly as the 3D master structure for the mold. Remarkably, master molds for PDMS are traditionally produced by photo- or electron-beam lithography followed by pattern transfer by plasma etching.[15] However, the resulting depth of plasma-etched features largely depends on the pattern geometry and density due to a micro-loading effect,[28,29] and is thus difficult to control. For the same reason, the rate of plasma etching is often non uniform across the etched substrate. Also, the resulting side wall profile of the etched features largely depends on the plasma conditions, and is also difficult to control. All these constrains severely complicate fabrication of plasma etched master molds. Here, we show that these constrains can be avoided by using a mold whose relief features are made of a patterned resist: not only such a mold eliminates the need of plasma etching, but it also ensures uniform relief features whose vertical dimensions are precisely controlled by the resist thickness. To that end, we patterned a photoresist film whose thickness was 1.6 µm to obtain relief features on the mold with 1.6 µm height.

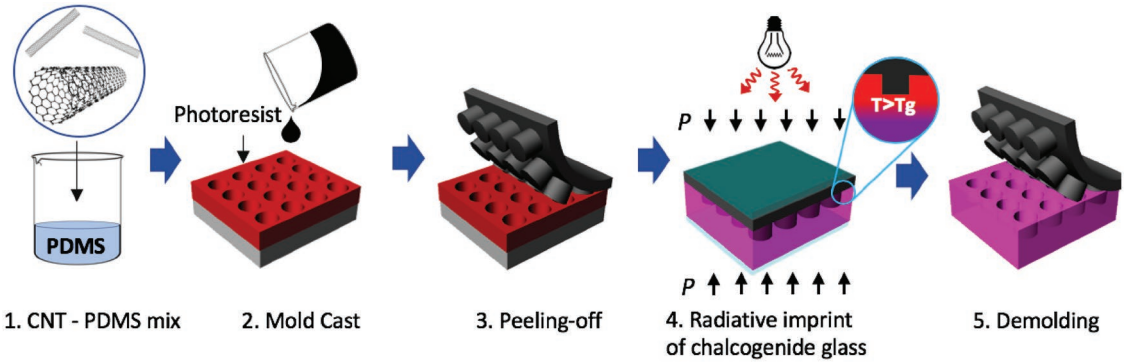

Figure 1. Process flow of direct radiative imprint of chalcogenide glass.

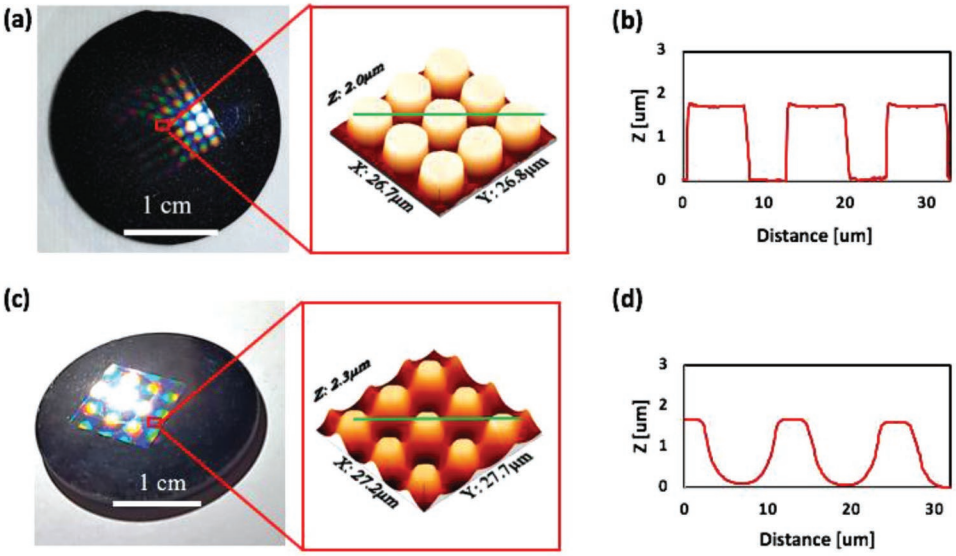

Figure 2. a) Carbon nanotube-PDMS composite mold, including 3D AFM of the pattern. b) Profile of the mold pattern. c) Imprinted As_2Se_3, including 3D AFM of the pattern. d) Profile of the imprinted pattern.

The key aspect of radiative imprint is the heating by a radiative source. Such heating requires that either mold or imprinted substrate would absorb the radiation. Notably, both As_2Se_3 (as most chalcogenide glasses) and PDMS—the material of choice for soft imprint molds—are transparent to the wavelength range of the radiative heating sources used in a nanoimprint equipment. To address this constrain and allow effective heat absorption of the soft mold, we reinforced PDMS with multiwall carbon nanotubes. Carbon nanotubes are ideal candidates for an adsorbing medium due to several reasons: i) their radius is a few orders of magnitude smaller than the relief features of the master mold, so they can easily fill these features without distorting the produced pattern; ii) carbon nanotubes are mechanically flexible, and iii) they effectively absorb light in the visible and near IR spectrum. Here, we cast a mixture of PDMS and multiwall carbon nanotubes directly onto a silicon wafer with patterned photoresist, baked it, and mechanically peeled it off the master. (see experimental section for details). The dimensions of the relief features on the obtained (**Figure 2**a) mold precisely replicated the pattern of the used master mold. In particular, their height (1.6 µm) exactly corresponded to the thickness of the photoresist used to structure the master mold.

Full pattern transfer from the mold to the imprinted surface is the main measure for a successful imprint process. In thermal imprint, full pattern transfer is achieved by heating the imprinted material to such a temperature that it is fluid enough to fill the mold relief within a reasonable time. Here, we radiatively heated the interface between As_2Se_3 and the mold, by keeping the mold temperature at 220 °C, which was monitored by a thermocouple that touched the membrane on the mold side. We assume, that due to the very effective heat transfer of carbon-nanotube reinforced PDMS,[30] the same temperature was maintained during the imprint at the mold-glass interface. While heated to such a temperature, As_2Se_3 reduces its viscosity to 10^8 Pa*s,[31] which is low enough for its imprint.[23] Figure 2b presents the resulting nanoimprinted surface of As_2Se_3. It can be clearly seen, that the depth of imprinted features corresponds to the height of the features in the mold, confirming that we indeed achieved full pattern transfer.

A remarkable advantage of radiative heating in the imprint process is that it allows fast heating to the desired temperature, usually within a few seconds. In our setup, the heating source faced the back side of the mold. Since carbon nanotube-PDMS composite is an effective thermal conductor, we believe that AS_2Se_3 surface reached the imprint temperature immediately after beginning the heating. We kept the total imprint time equal to 4 min. We believe that this imprint time was long enough to achieve full pattern transfer, but short enough to prevent the deformation of the bulk of the As_2Se_3 substrate. Such a tight control over the imprint time enabled to maintain the original shape and dimensions of the As_2Se_3 substrate. To quantitatively asses the possible impact of imprint on the global shape of As_2Se_3 substrate, we characterized its flatness by profilometry and 2D laser scanning. We found, that As_2Se_3 developed a bow of about 150 µm, which is due to the creep that As_2Se_3 undergrows at the temperature and pressure used in our process (**Figure 3**a–c). To prevent this creep, we attached a flat (flatness < 1 µm) BK7 glass substrate to the backside of the As_2Se_3 substrate (Figure 3d). Both profilometry (Figure 3c) and laser scanning (Figure 3e) of the As_2Se_3 substrate which was supported by BK7 during the imprint showed a near zero bow, and a small warpage (measure of localized deviation from complete flatness) comparable to that of a pristine unimprinted As_2Se_3 substrate.

Maintaining the structure and composition of chalcogenide glasses during their imprint is critical for their optical application. It was previously shown, for example, that chalcogenide glasses such as As_2S_3 crystalize upon their imprint.[32,33] As for As_xSe_{1-x} glasses, their bulk-nucleation and crystallization that occurs during the thermal cycles was fundamentally investigated,[34,35] and found to be dependent on As content and the impurities present in the glass. Importantly, crystallization of

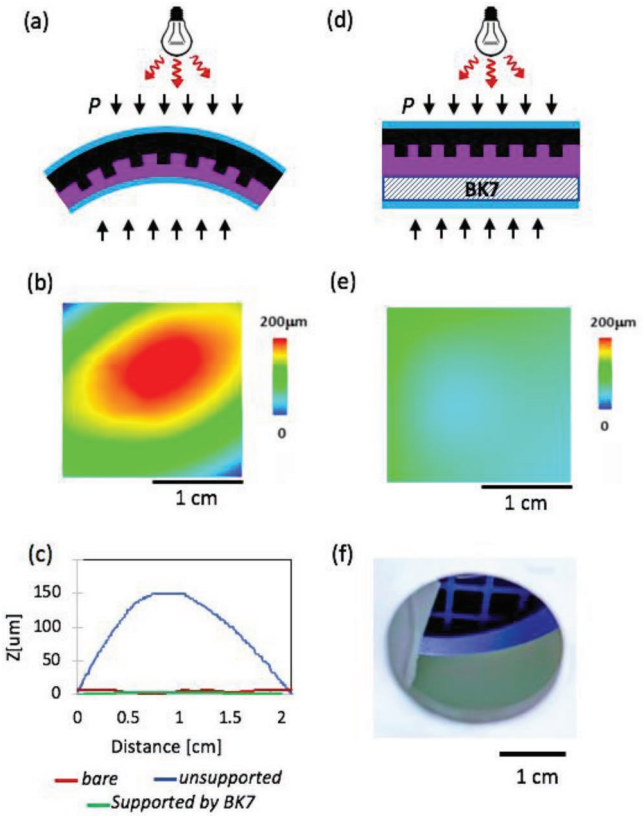

Figure 3. a) Scheme of the bow generation in imprinted As_2Se_3 substrate. b) 2D laser scanning of imprinted As_2Se_3. c) Profilometry scans of bare and imprinted As_2Se_3 substrates. d) Scheme of the imprint configuration in which As_2Se_3 is supported by BK7 glass. e) 2D laser scanning As_2Se_3 imprinted with the back side support of BK7 glass. f) Photography image of the backside of As_2Se_3 substrate imprinted with BK7 support.

nanoimprinted chalcogenide glass is highly undesirable for optical applications because of the high scattering loss caused by the crystalline domains. To assess whether our imprint process causes any crystallization of As_2Se_3, we characterized the imprinted surface by X-ray Electron Diffraction ($\lambda_{CuK\alpha}$ = 0.1542 nm) (**Figure 4**a). The measured spectrum shows a broad peaks characteristic of a completely amorphous structure of As_2Se_3,[36] and clearly demonstrate that our nanoimprint process does not cause crystallization.

We used additional characterization techniques to asses any possible effect of the nanoimprint process on the structure and composition of As_2Se_3. Figure 4b,c shows Raman spectrum of bare and imprinted As_2Se_3, respectively. The deconvolution of the main Raman peak produced five peaks that correspond to different vibrational modes of As_2Se_3. These peaks are broad for both As_2Se_3 before and after the imprint, which provides additional confirmation that no crystallization takes place upon the imprint process. We also calculated the areas of each peak, in order to assess possible changes in material structure (Figure 4d). Here, an increase in peak areas at 223 cm^{-1} that corresponds to the vibration of As_2Se_3 pyramidal unit, and of the peak at 241 cm^{-1} that corresponds to Se–Se chain, indicate an increase in the degree of crosslinking in the glass network. This observation mirrors previously reported Raman analysis of thermally imprinted As_2Se_3 thin film.[23] We believe that this increase in the relative amount of cross-linked As_2Se_3 caused the decrease of the peaks related to the non-crosslinked units, such as the peak at 212 cm^{-1} that corresponds to As_4Se_4 unit.

We also characterized bare and imprinted As_2Se_3 surfaces by X-ray Photoelectron Spectroscopy (XPS), as shown in Figure 4e,f. We found that in both cases the surface contained As and Se in stochiometric ratio (2:3). We also found a certain amount of oxygen. We performed XPS analyses at varying depths, using Ar sputtering (Figure 4g,h), and found that for both bare and imprinted As_2Se_3, oxygen was present only down to a ≈20 nm depth. Since the binding energies of As and Se peaks did not vary with the sampling depth, we conclude that oxygen signals originates from contaminations rather than from oxidized As and Se. Finally, we can see presence of silicon on the imprinted As_2Se_3 surface. The binding energy of Si was found to be 103 eV, which corresponds to one previously measured for Si2p in PDMS.[37] We thus conclude that both observed O and Si signals originate from a minor contamination caused by the contact with PDMS during imprint. We can further confirm that Si contamination is present only on the surface and not in the bulk of As_2Se_3, based on EDS of bare and imprinted substrates (Figure 4i). According to EDS, which represents the composition averaged over about 1 μm depths, the stochiometric ratio between As and Se is maintained throughout the imprint. This finding mirrors previously discussed XPS results. Also, elements such as Si, O, and C appear in negligible amount, confirming that they originate from the PDMS surface contamination. Finally, we used AFM to characterize the roughness of the imprinted surface, which can be evaluated as the standard deviation (STD) of the surface 2D height profile. We found that STDs of both bare and imprinted As_2Se_3 substrates are similar, and equal to 5 nm. Thus, nanoimprint does not produce any change in the substrate roughness.

To demonstrate the applicability of our imprint process in the fabrication of optical devices and components, we characterized the imprinted diffraction grating in two modes—reflective and transmitting. Since As_2Se_3 is reflective in the visible region, we used a HeNe laser (632.8 nm) as the light source for the characterization of reflective diffraction. The characterization setup consisted of a HeNe laser, whose beam passed through two apertures—a standard optical aperture used to reduce the beam diameter, and another aperture within a black board. The board, in turn, was used to visualize 2D diffraction pattern reflected form the imprinted As_2Se_3 (**Figure 5**a.) The sample tilt and rotation was aligned to ensure that the beam of the 0-order diffraction returns exactly into the aperture in the board. By measuring the distances between the laser spots in the obtained diffraction pattern, we calculated the diffraction angles (**Table 1**). We found that these angles are in a good agreement with the theoretical angles, which were calculated from the relation between the diffraction angle and the grating geometry: $d \sin \theta = n\lambda$, ($n = 0, \pm1, \pm2...$). Here d is the pattern periodicity, which was set at 8 μm in our calculations, according to the periodicity of the photolithographic mask used to prepare the master. This good agreement between the calculated diffraction angles and the diffraction angles measured in both x and y direction confirms that the grating geometry was faithfully reproduced from the master to the imprinted surface.

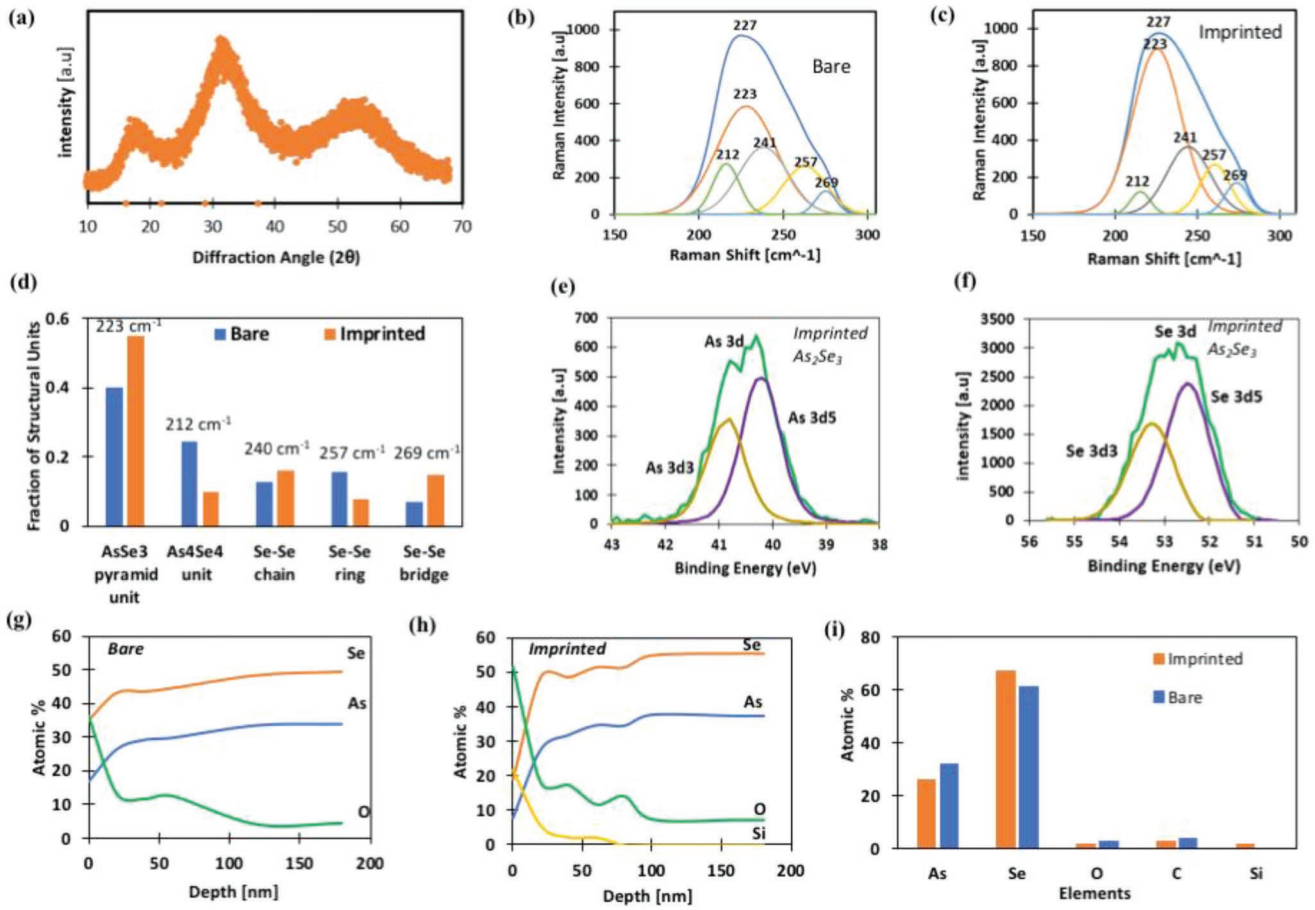

Figure 4. Material analysis of bare and imprinted As_2Se_3. a) XRD of imprinted sample, showing amorphous structure of As_2Se_3. b) and c) Raman peaks of bare and imprinted substrates, respectively. d) Fraction of Raman structural units. e) and f) Deconvolution of XPS As and Se peaks obtained for imprinted As_2Se_3. g) and h) XPS based analysis of elements ad different depth for bare and imprinted As_2Se_3, respectively. i) EDS based material analysis for bare and imprinted As_2Se_3.

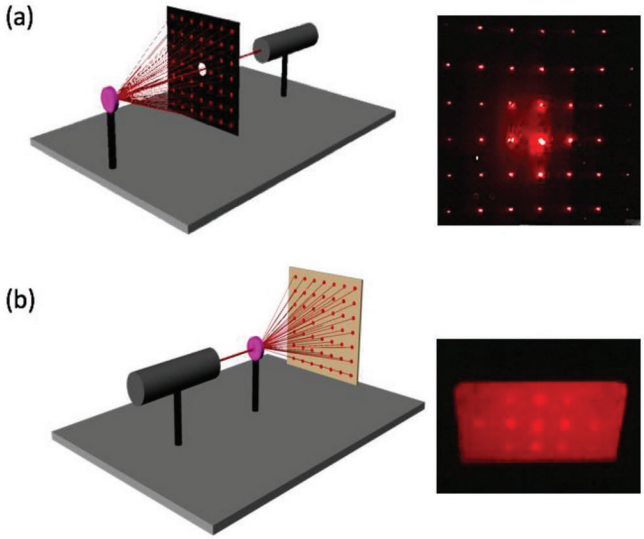

Figure 5. Characterization of diffraction grating directly imprinted in As_2Se_3. a) Scheme of measurement setup and reflection diffraction pattern obtained using HeNe laser. b) Scheme of measurement setup and transmission diffraction pattern obtained using HeNe laser.

Such a high pattern fidelity indicates that our process holds great potential for the fabrication of precision optics based on chalcogenide glasses.

As_2Se_3, as well as many other chalcogenide glasses, is an attractive material for near IR and mid IR optics, due to its high refractive index, as well as high transparency and low levels of optical losses, in this range of wavelengths. To demonstrate the applicability of our novel imprint approach for the fabrication of IR optical components, we characterized the fabricated grating in transmission mode. Here, the IR laser (1550 nm) was pointed to the backside of the imprinted As_2Se_3 substrate, and the diffraction pattern was visualized on the infrared detection card positioned in front of the sample (Figure 5b). Similarly to what was observed in reflection mode, here the measured

Table 1. Calculated and measured angles for reflection diffraction grating.

Diffraction order	±1	±2	±2
Calculated angle	3.6°	7.3°	10.9°
Angle measured in *x* direction	3.8°	7.6°	11.6°
Angle measured in *y* direction	3.8°	7.6°	11.6°

Table 2. Calculated and measured angles for transmission diffraction grating.

Diffraction order	±1	±2
Calculated angle	8.5°	18.4°
Angle measured in *x* direction	9.5°	17.6°
Angle measured in *y* direction	9.5°	17.6°

diffraction angles were also in good agreement with the calculated ones (**Table 2**).

Whereas different lithographic approaches can be applied to produce functional structures on the surface of chalcogenide glasses, all of these are fundamentally limited to flat surfaces. Patterning of curved substrates, such as lenses, is still a challenge. In this context, the great advantage of soft imprint is in its applicability to curved substrates. Still, imprint on curved surfaces was applied so far to pattern thin polymeric films on solid curved substrates.[17,38] At the time, direct imprint of a curved surface of any material has never been demonstrated. Here, we show the applicability of our imprint process to pattern optical surfaces of chalcogenide glasses with a non-planar geometry, by producing a diffraction grating on a lens of As_2Se_3, with a diameter of 50 cm and radius of curvature of 43 mm. **Figure 6** shows a typical diffraction grating on a As_2Se_3 lens. The AFM images of this grating clearly demonstrate that the imprinted pattern faithfully replicates the geometry of the master mold. Notably, we measured the grating period at the pattern center and its periphery (5 mm from the center). We found that the period at the periphery is 6% larger than that of the master mold. We believe that this increase in the imprinted period stems from the necessary mold stretching to form a uniform and conformal contact with the curved surface of the lens. We also believe that this stretching effect can be compensated by an appropriate mold design, in which the periodicity is deliberately reduced from the center to its periphery. To the best of our knowledge, this is the first time direct imprint of non-planar surface of chalcogenide glass has been demonstrated.

In summary, we report a novel approach for the direct surface pattering of chalcogenide glasses. The uniqueness of our approach is that it allows the facile and robust thermal forming of miniaturized structures on the surface with full pattern transfer from the elastomeric mold to the glass surface, and, at the same time, to maintain the original shape of the imprinted substrate. Compared to the state-of-the art serial approaches for the nanopatterning of chalcogenide gasses, such as laser or electron-beam writing, our approach is massively parallel—one imprint process takes a few minutes, independently of the pattern area—and allows scalable high throughput fabrication of light manipulating structures. The extensive material characterization confirms that the composition and structure of imprinted As_2Se_3 are well maintained throughout the imprint process. Thus, the imprint can be applied to the fabrication of optical devices and components without compromising on the optical performance of the imprinted material. We further demonstrated the broad potential of our fabrication process by directly imprint and characterizing the diffraction grating on the surface of As_2Se_3. Furthermore, there is a broad variety of chalcogenide glasses whose glass transition point is in the same range as that of As_2Se_3 (e.g., T_g of As_2S_3 is 185 °C and T_g of $GeSe_4$ is 163 °C[19]), therefore we believe that these glasses can be thermally imprinted similarly to As_2Se_3, and we intend to explore direct nanoimprint of a few of them in the near future.

Finally, we patterned the surface of a lens, and thus showed the great potential of our approach for producing light-manipulating structures on surfaces with unconventional, non-planar geometries. Such surfaces include, for instance, lenses, as well as free-form optical surfaces tailored for specific applications. Overall, our novel approach paves the way for numerous applications of chalcogenide glass in miniaturized optical devises, whose structural and functional complexity is unachievable today.

Experimental Section

PDMS- nanotube composite mold: Multiwall Carbon Nanotubes (Cheep Tubes Inc.) were first dispersed in toluene using a probe sonicator. In parallel, PDMS (Sylgard 184, Dow Corning) was diluted in toluene (2:1) and was placed in an ultrasonic bath for 1 h. The two solutions were mixed and sonicated in a probe sonicator for 1 h. The mixture was then placed in a rotary evaporator for the evaporation of the toluene from the solution.[39,40] Finally, a curing agent was added to the PDMS-MWCNT solution and manually mixed for 10 min. The solution was then cast onto the master mold, degassed, and baked.

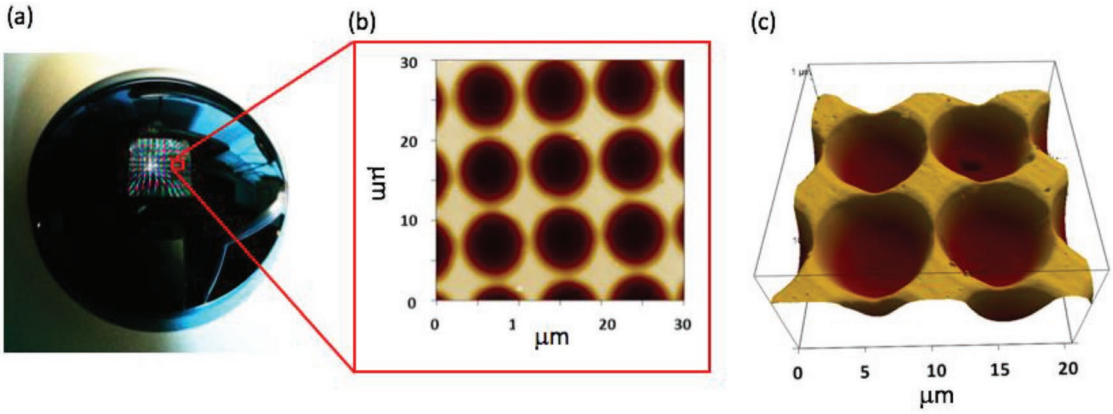

Figure 6. a) Diffraction grating imprinted on the surface of As_2Se_3 lens, (b) and (c) top view and 3D AFM of the imprinted diffraction grating.

Nanoimprint: 2.5 cm circular substrates of As_2Se_3 were imprinted in a commercial nanoimprint tool (Nanonex NX-B200). The mold was placed on the bottom, facing the radiative source. The imprint temperature was 220 °C (which was monitored throughout the imprint process by a thermocouple touching the membrane on the mold side). The imprint pressure was 50 psi, and the imprint time 4 min. The convex lens was imprinted using the same conditions as the flat substrates.

Characterization of imprinted As_2Se_3: The flatness of bare and imprinted substrates was measured by profilometry (Veeco Dektak 8), and laser profiler OLS5000. XRD was measured using Rigaku, D/max-2100, Cu(kα), 40 keV, 30 mA. Raman Spectroscopy was measured using Horiba LabRam HR evolution micro-Raman system, equipped with a Synapse Open Electrode CCD detector air-cooled to –60 °C. The excitation source was a 532 nm laser with a power on the sample of 0.05 mW, and typical exposure of 180 s. Notably, this power of laser is very low compared to that previously reported for the characterization of imprinted As_2Se_3,[23] and it was intentionally chosen by us to ensure that no structural or compositional changes are caused to As_2Se_3 during the Raman measurement. The laser was focused with an x50 objective to a spot of about 2 µm. The measurements were taken with a 600 g mm^{-1} grating and a 100 µm confocal microscope hole. XPS data were collected using an X-ray photoelectron spectrometer ESCALAB 250 ultrahigh vacuum (1×10^{-9} bar) apparatus with an AlK^{α} X-ray source and a monochromator. The X-ray beam size was 500 µm and survey spectra were recorded with pass energy (PE) 150 eV and high energy resolution spectra were recorded with a pass energy (PE) 20 eV. To correct for charging effects, all spectra were calibrated relative to a carbon C 1s peak positioned at 284.8 eV. Processing of the XPS results was carried out using AVANTGE program.

Conflict of Interest

The authors declare no conflict of interest.

Keywords

carbon nanotubes, chalcogenide glasses, nanoimprint, soft imprint

Received: April 18, 2019
Revised: June 19, 2019
Published online:

[1] L. Li, H. Lin, S. Qiao, Y. Zou, S. Danto, K. Richardson, J. D. Musgraves, N. Lu, J. Hu, *Nat. Photonics* **2014**, *8*, 643.
[2] C. R. Petersen, U. Møller, I. Kubat, B. Zhou, S. Dupont, J. Ramsay, T. Benson, S. Sujecki, N. Abdel-Moneim, Z. Tang, D. Furniss, A. Seddon, O. Bang, *Nat. Photonics* **2014**, *8*, 830.
[3] H. Lin, Y. Song, Y. Huang, D. Kita, S. Deckoff-Jones, K. Wang, L. Li, J. Li, H. Zheng, Z. Luo, H. Wang, S. Novak, A. Yadav, C.-C. Huang, R.-J. Shiue, D. Englund, T. Gu, D. Hewak, K. Richardson, J. Kong, J. Hu, *Nat. Photonics* **2017**, *11*, 798.
[4] L. G. Aio, A. M. Efimov, V. F. Kokorina, *J. Non-Cryst. Solids* **1978**, *27*, 299.
[5] H. Nasu, K. Kubodera, M. Kobayashi, M. Nakamura, K. Kamiya, *J. Am. Ceram. Soc.* **1990**, *73*, 1794.
[6] G. B. Hoffman, W.-C. Liu, W. Zhou, R. Sooryakumar, P. Boolchand, R. M. Reano, *J. Vacuum Sci. Technol. B: Microelectr. Nanometer Struct.* **2008**, *26*, 2478.
[7] E. V. Berlin, B. T. Kolomiets, V. M. Lyubin, S. I. Nesterov, V. V. Rudnev, V. P. Shilo, *Sov. Tech. Phys. Lett* **1981**, *7*, 654.
[8] V. Lyubin, *Physica Status Solidi B* **2009**, *246*, 1758.
[9] M. Wuttig, H. Bhaskaran, T. Taubner, *Nat. Photonics* **2017**, *11*, 465.
[10] S. Schroeter, M. Vlček, R. Poehlmann, A. Fišerová, *J. Phys. Chem. Solids* **2007**, *68*, 916.
[11] J. Wei, X. Jiao, *Proc. SPIE* **2008**, *7125*, 712505.
[12] A. Zoubir, M. Richardson, C. Rivero, A. Schulte, C. Lopez, K. Richardson, N. Hô, R. Vallée, *Opt. Lett.* **2004**, *29*, 748.
[13] J. Teteris, M. Reinfelde, *J. Non. Cryst. Solids* **2007**, *7*, 127.
[14] A. Kovalskiy, *J. Micro/Nanolithography, MEMS, MOEMS* **2009**, *8*, 043012.
[15] T. W. Odom, J. C. Love, D. B. Wolfe, K. E. Paul, G. M. Whitesides, *Langmuir* **2002**, *18*, 5314.
[16] D. Morecroft, J. K. W. Yang, S. Schuster, K. K. Berggren, Q. Xia, W. Wu, R. S. Williams, *J. Vacuum Sci. Technol. B: Microelectr. Nanometer Struct.* **2009**, *27*, 2837.
[17] V. Bhingardive, L. Menahem, M. Schvartzman, *Nano Res.* **2018**, *11*, 2705.
[18] A. Pandey, S. Tzadka, D. Yehuda, M. Schvartzman, *Soft Matter* **2019**, *15*, 2897.
[19] V. S. Shiryaev, M. F. Churbanov, in *Chalcogenide Glasses: Preparation, Properties and Applications* (Eds: J.-L. Adam, X. Zhang), Woodhead Publishing Ltd., Cambridge, UK **2014**, pp. 3–35.
[20] T. Han, S. Madden, D. Bulla, B. Luther-Davies, *Opt. Express* **2010**, *18*, 19286.
[21] M. Solmaz, H. Park, C. K. Madsen, X. Cheng, *J. Vacuum Sci. Technol. B: Microelectr. Nanometer Struct.* **2008**, *26*, 606.
[22] S. Danto, E. Koontz, Y. Zou, T. O. Ogbuu, B. Gleason, P. Peter Wachtel, J. D. Musgraves, J. Hu, K. Richardson, *Proc. SPIE* **2013**, *9884*, 88841T.
[23] Y. Zou, D. Zhang, H. Lin, L. Li, L. Moreel, J. Zhou, Q. Du, O. Ogbuu, S. Danto, J. D. Musgraves, K. Richardson, K. D. Dobson, R. Birkmire, J. Hu, *Adv. Opt. Mater.* **2014**, *2*, 478.
[24] J. Orava, T. Kohoutek, L. Greer, H. Fudouzi, *Opt. Mater. Express* **2011**, *1*, 796.
[25] M. R. Lotz, C. R. Petersen, C. Markos, O. Bang, M. H. Jakobsen, R. Taboryski, *Optica* **2018**, *5*, 557.
[26] D. Yehuda, E. Kassis, S. Joseph, M. Schvartzman, *J. Vacuum Sci. Technol. B* **2018**, *36*, 031602.
[27] R. Blachnik, A. Hoppe, *J. Non-Cryst. Solids* **1979**, *34*, 191.
[28] C. Hedlund, *J. Vacuum Sci. Technol. B: Microelectr. Nanometer Struct.* **1996**, *14*, 3239.
[29] M. C. Elwenspoek, H. V. Jansen, *Silicon Micromachining*, Cambridge University Press, Cambridge, UK **1999**.
[30] S. Y. Kwon, I. M. Kwon, Y.-G. Kim, S. Lee, Y.-S. Seo, *Carbon* **2013**, *55*, 285.
[31] J. D. Musgraves, P. Wachtel, S. Novak, J. Wilkinson, K. Richardson, *J. Appl. Phys.* **2011**, *110*, 063503.
[32] K. Richardson, D. Krol, K. Hirao, *Int. J. Appl. Glass Sci.* **2010**, *1*, 74.
[33] B. J. Eggleton, B. Luther-Davies, K. Richardson, *Nat. Photonics* **2011**, *5*, 141.
[34] A. Giridhar, S. Mahadevan, A. K. Singh, *Bull. Mater. Sci.* **1987**, *9*, 13.
[35] M. Kitao, C. Gotoh, S. Yamada, *J. Mater. Sci.* **1995**, *30*, 3521.
[36] J. A. Frantz, J. D. Myers, R. Y. Bekele, C. M. Spillmann, J. Kolacz, H. Gotjen, V. Q. Nguyen, C. C. McClain, J. S. Sanghera, *Opt. Mater. Express* **2018**, *8*, 3659.
[37] P. Louette, F. Bodino, J.-J. Pireaux, *Surf. Sci. Spectra* **2005**, *12*, 1.
[38] Z. Li, Y. Gu, L. Wangs, H. Ge, W. Wu, Q. Xia, C. Yuan, Y. Chen, B. Cui, R. S. Williams, *Nano Lett.* **2009**, *9*, 2306.
[39] M. I. Shahzad, M. Giorcelli, N. Shahzad, S. Guastella, M. Castellino, P. Jagdale, A. Tagliaferro, *J. Phys.: Conf. Ser.* **2013**, *439*, 012010.
[40] S. Pyo, J.-I. Lee, M.-O. Kim, T. Chung, Y. Oh, S.-C. Lim, J. Park, J. Kim, *J. Micromech. Microeng.* **2014**, *24*, 075012.

